J Mater Sci: Mater Electron (2022) 33:8159–8170

GaSb/Mn multilayers structures fabricated by DC magnetron sputtering: Interface feature and nano-scale surface topography

Jorge A. Calderón[1], Heiddy P. Quiroz[1,*], M. Manso-Silván[2], Álvaro Muñoz Noval[3], A. Dussan[1], and H. Méndez[4]

[1] *Dpto. de Física, Grupo de Materiales Nanoestructurados Y Sus Aplicaciones, Universidad Nacional de Colombia - Bogotá, Cra. 30 No. 45-03 Edificio 404 Yu Takeuchi Lab. 121C / 121B-1 Ciudad Universitaria, 110001 Bogotá, Colombia*

[2] *Departamento de Física Aplicada, Instituto de Ciencia de Materiales Nicolás Cabrera Y Centro de Microanálisis de Materiales, Universidad Autónoma de Madrid, 28049 Madrid, Spain*

[3] *Departamento de Física de Materiales. Facultad de Ciencias Físicas, Universidad Complutense de Madrid, Plaza de Ciencias, 1, 28040 Madrid, Spain*

[4] *Physics Department, Science Faculty, Pontificia Universidad Javeriana, Bogotá D.C, Colombia*

Received: 3 September 2021
Accepted: 16 February 2022
Published online: 5 March 2022

© The Author(s), under exclusive licence to Springer Science+Business Media, LLC, part of Springer Nature 2022

ABSTRACT

The multilayer structure is a well-studied architecture for electronic and optoelectronic applications and more recently in spintronic devices. In this work, we present the structural, morphological, topographical, and magnetic properties of GaSb/Mn multilayers deposited via DC magnetron sputtering at room temperature and 423 K. Raman measurements evidence the formation of p-type GaSb layers with a contribution of electrons in the multilayer due to the neighboring Mn layer and the formation of effective interlayers. HR-SEM measurements show the multilayer architecture with columnar microstructure in the layer's formation, while AFM micrographs allowed observing the changes in grain sizes (between 129 and 187 nm) and roughness (between 1.47 nm and 6.28 nm) with increasing number of layers. The formation of the interlayers between the GaSb and Mn layer was assayed in-depth spectroscopically via Rutherford backscattering studies. These interlayers were associated with diffusion processes during deposition and contributed to the magnetic behavior of multilayers. A ferromagnetic-like behavior was observed in the multilayers.

Address correspondence to E-mail: hpquirozg@unal.edu.co

https://doi.org/10.1007/s10854-022-07965-9

1 Introduction

Multilayer thin films are architectures formed by layers of two or more materials based on transition elements, semiconductors, or alloys [1–3]. The magnetic and electrical properties of these structures can be modified through the thickness, diffusion process, and distribution of the metal layers [4]. Synthesis methods and fabrication parameters affect multilayer growth and play a determinant role in thin films' topography and interface diffusion [4]. Based on these features, potential applications of multilayers have been reported as quantum nanodots for optoelectronics [5], electronic devices [6], and magnetic storage technology [7], among others. The synthesis methods for these types of system include Molecular Beam Epitaxial (MBE) [8, 9], Radio Frequencies (RF) magnetron co-sputtering [10], Metalorganic Chemical Vapor Deposition (MOCVD) [11], and the most recent DC magnetron sputtering [11]. The advantage of this last synthesis method, with respect to others such as MBE, is the reduction in manufacturing costs maintaining quality in the crystalline properties of the GaSb compound, the growth control, and the homogeneity of the layers, among others. Among the properties of multilayer systems manufactured by MBE, the obtaining of p-type GaSb [8] and heterointerfaces of As and Sb between the formation of InAs/GaSb layers [9] have been reported.

GaSb is a semiconductor with a band gap of 0.72 eV [12, 13] that is used in electronic devices [12], photovoltaic cells, and quantum dots [14]. From these studies, research of III–V compounds based on heterostructures has derived to systems such as InAs/GaSb acting as photon traps [15], Sb/GaSb acting as narrow band-gap structures [12], and GaSb/GaAs acting as absorbing/emitting quantum dots [16]. Due to the electrical properties of GaSb associated with gallium (V_{Ga}) and antimony (V_{Sb}) vacancies and the role of growth mechanism [17], the study of defects, interface effects, and growth of multilayer architecture is necessary for the promotion of device quality.

In this work, we present a study of the growth mechanism, topographic features, and morphological characterization through Raman and HR-SEM measurements of GaSb/Mn multilayer system deposited via DC magnetron sputtering at room temperature. We additionally proposed to study the effect on defects at the interface through in-depth Rutherford Backscattering Spectroscopy (RBS) analysis. We further study the multilayers magnetic behavior at room temperature as a function of the thickness of the Mn and GaSb layers.

2 Experimental methods

2.1 Synthesis parameters

GaSb/Mn multilayer thin films were fabricated via DC magnetron sputtering using $Ga^{(36.5\%)}Sb^{(63.5\%)}$ (99.995% purity) and Mn (99.9% purity) targets in Argon atmosphere at 2.5×10^{-2} Torr working pressure. These samples were deposited at room temperature on Si (001) and GaSb (001) wafer substrates. An alternation between GaSb target power and Mn target power was implemented. First, for 20 min, GaSb was deposited by applying 100 W, and then the GaSb target power was turned off, and simultaneously, the Mn target power was turned on for 15 min applying 60 W of target power. This process was repeated for 3 and 6 times to obtain the samples with 3 and 6 periods, called as $[GaSb/Mn]_3$ and $[GaSb/Mn]_6$, respectively, with substrate temperature (Ts) of 293 K and 423 K.

2.2 Characterization techniques

Structural identification was carried out by Raman measurements performed at room temperature, using a laser of λ_e = 532 nm and 633 nm, with an exposure time of 1000 ms maintaining a beam configuration perpendicular to the sample, through the 50X optical lens given by the Renishaw InVia Raman Microscope.

Cross-sectional and topographic characterizations of the multilayers were carried out on a FEI VERIOS 460 Scanning Electron Microscope with a maximal resolution of 0.6 nm at 15 kV at high vacuum regime ($\sim 10^{-6}$ mbar). The cross section was realized to 80° of inclination. An Atomic Force Microscopy Asylum Research MFP 3D Bio in tapping mode was used. On the other hand, Rutherford Backscattering Spectroscopy was performed using a Cockroft-Walton tandem-linear accelerator with He + particles with energy of 2 MeV and 3.035 MeV. Planar Si detectors collect the backscattered particles from the sample at an angle of 170° with normal incidence. The RBS

analysis was performed using the SIMNRA simulation software package [18].

Hall and resistivity measurements at room temperature were performed with a Hewlett Packard 4041B Source and meter unit controlled by the software National Instruments LabVIEW for data acquisition. The magnetic field applied was $B = 1.09 \pm 0.05T$.

3 Analysis and results

Figure 1 shows XRD patterns and Raman spectra of $[GaSb/Mn]_3$ obtained for 532 nm and 633 nm excitation for multilayers with Ts = 293 K and 423 K. In the Raman spectra (Fig. 1a and Fig. 1b), the formation of the p-type GaSb was identified. This is due to the fact that a qualitative relationship between the coupled-mode spectral characteristics and the concentration of holes has been reported from Raman spectroscopic studies on p-type GaSb and p-type GaAs. In both cases, as the concentration of holes increases, the linewidth of the coupled mode of the accumulation layer widens and the peak wave number decreases with respect to the LO phonon mode (236 cm^{-1}) [19–22]. Figure 1a and b shows the decrease of the LO mode with peaks located at 225.34 cm^{-1} and 232.03 cm^{-1} for 532 nm excitation, and at 226.72 cm^{-1} and 235.89 cm^{-1} for 633 nm excitation. Therefore, p-type GaSb fabricated via DC magnetron sputtering exhibits a hole accumulation layer (according Ref. [22]) which may be described for the depletion Surface Space Charge Region (SSCR) observed in the interaction of Longitudinal Optical (LO) and Transverse Optical (TO) modes at circa 230 cm^{-1} [19, 20].

In the Raman spectra (Fig. 1a and b), the formation of the p-type GaSb was identified, since a qualitative

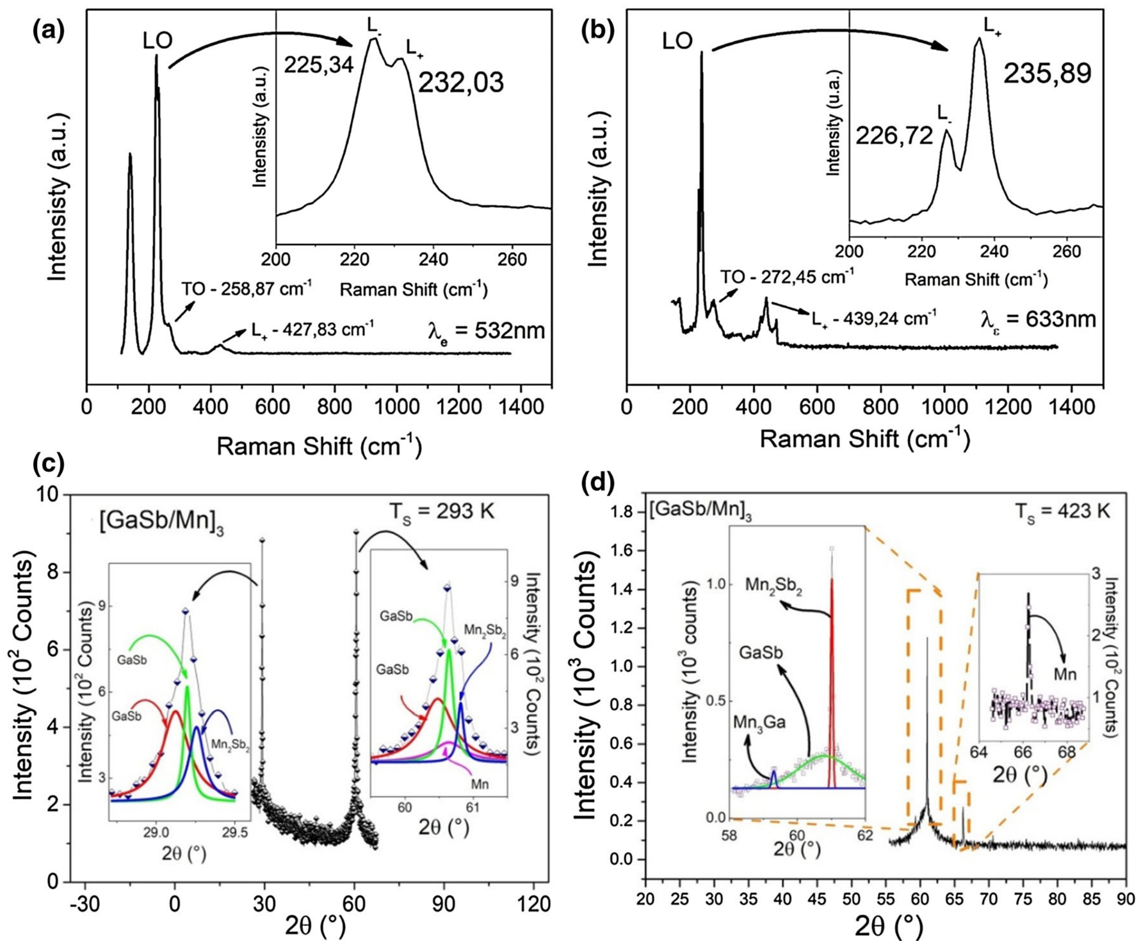

Fig. 1 Raman spectra of $[GaSb/Mn]_3$ multilayer at Ts = 293 K obtained for **a** 532 nm, and **b** 633 nm excitation. XRD patterns for GaSb/Mn multilayer samples with n = 3 and substrate temperature at **c** 293 K and **d** 423 K

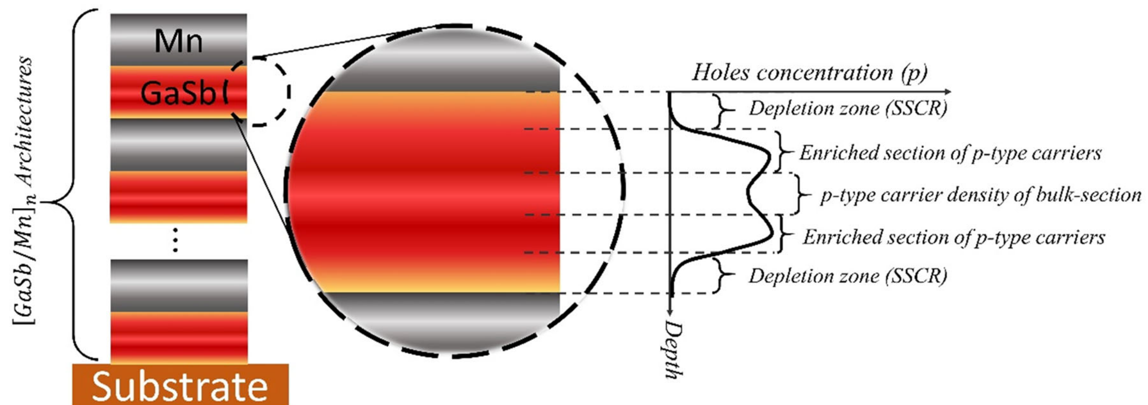

Fig. 2 Scheme of Surface Space Charge Region (SSCR) and virtual layers

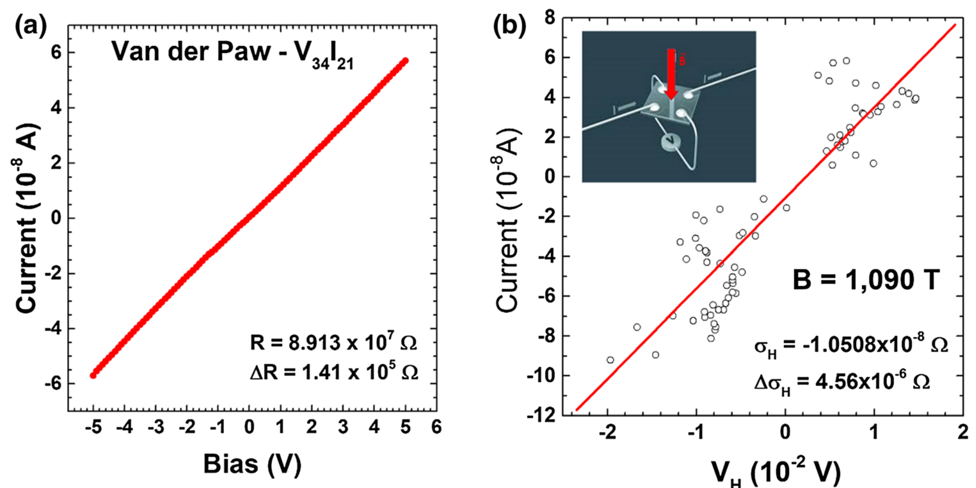

Fig. 3 **a** Individual I-V measurement for estimating resistivity using Van der Pauw configuration, and **b** Current as a function of Hall voltage plot for deducing film's Hall conductance of $[GaSb/Mn]_3$ multilayer with Ts = 423 K. Inset shows the selected configuration for performing Hall effect measurements

relationship between the coupled-mode spectral characteristics and the concentration of holes has been reported in Raman spectroscopic studies on p-type GaSb and p-type GaAs. In both cases, as the concentration of holes increases, the linewidth of the coupled mode of the accumulation layer widens and the peak wave number decreases with respect to the LO phonon mode (236 cm^{-1}) [14–17]. Figure 1a and b shows the decrease of the LO mode with peaks located at 225.34 cm^{-1} and 232.03 cm^{-1} for 532 nm excitation, and at 226.72 cm^{-1} and 235.89 cm^{-1} for 633 nm excitation. Therefore, p-type GaSb fabricated via DC magnetron sputtering exhibits a hole accumulation layer (according to [18]), which may be described for the depletion Surface Space Charge Region (SSCR) observed in the interaction of Longitudinal Optical (LO) and Transverse Optical (TO) modes at circa 230 cm^{-1} [14, 15].

For 532 nm excitation (Fig. 1a), it is possible to observe the presence of two coupled phonon–plasmon modes with a Raman shift of 225.34 cm^{-1} (low-frequency mode (L_-)) and 232.03 cm^{-1} (high-frequency mode (L_+)). However, it has been reported that the L_+ mode wavenumber increases from 236 cm^{-1} to 620 cm^{-1} with increasing electron concentration [19, 20]. In our case, the formation of Mn layers and ions diffusion at the interfaces contributed to the increase of the L_+-band Raman shift. Hence, in Fig. 1a, the presence of the peak around 427.83 cm^{-1} is associated to the high-frequency mode. In comparison, decreasing the excitation energy to 633 nm (Fig. 1b) shows the low-frequency mode at 226.72 cm^{-1}, whereas the high-frequency mode increases in intensity and is located in 235.89 cm^{-1} and 439.24 cm^{-1}.

The depletion SSCR suggests the presence of an in-depth gradient that can be explained that considering a virtual three-layer model, for the interaction between excitation wavelength and material (see Fig. 2): first, the bulk with a given concentration of

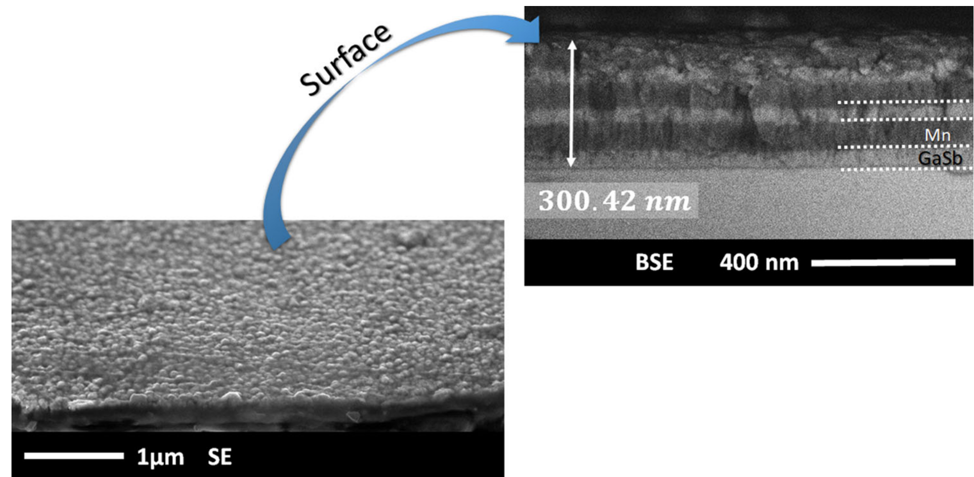

Fig. 4 HR-SEM micrographs of surface and cross section of $[GaSb/Mn]_3$ multilayer on GaSb wafer at Ts = 293 K

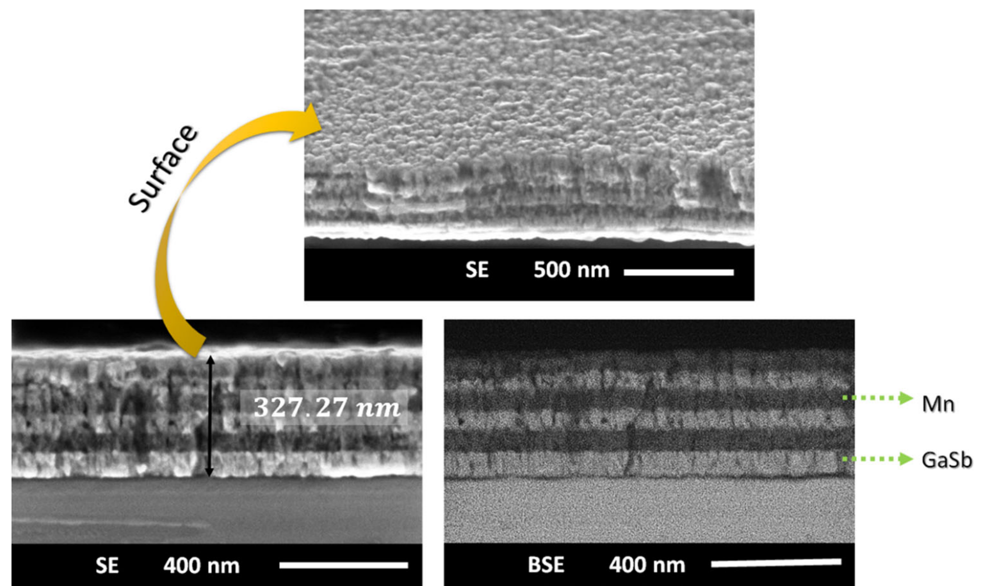

Fig. 5 HR-SEM micrographs of the surface and cross section of $[GaSb/Mn]_3$ multilayer on GaSb wafer at Ts = 423 K

hole (from the interior of the virtual layer towards the surface); then, a layer between the surface and the bulk that is enriched in hole concentration relative to the bulk; finally, a surface virtual layer with no hole concentration (near the surface of the thin film) (Fig. 2). Therefore, depending on the excitation source, the LO phonon-hole plasmon coupled-mode scattering is originated from the bulk of the material and hole-enriched layer, while LO phonon mode scattering is originated from the hole-depleted near-surface layer [19].

In addition, Fig. 1c and d shows the XRD patterns for GaSb/Mn multilayer samples with n = 3 and substrate temperature at 293 and 423 K. The shape of peaks presents shoulders and asymmetric characteristics, which were deconvoluted using Lorentzian functions for each crystalline phase contribution. Through Rietveld method, the GaSb (PDF 00–007-0215 and PDF 01–088-2490), Mn_2Sb_2 (PDF 96–900-8590), Mn_3Ga (PDF 00–037-0913), and Mn-α (PDF 96–900-8590) phases were identified. From Fig. 1 d, we can observe that Mn_3Ga and Mn_2Sb_2 phases formation has been generated due to the increase of substrate temperature. The GaSb, Mn_2Sb_2, and Mn- α crystalline phase formation at room temperature is a particularly relevant result since the reduction of CO_2 traces in Electronics Engineering should be a mandatory objective in all manufacturing processes, as in general, they use high synthesis temperatures between 413 and 873 K [23–25].

On the other hand, the standard van der Pauw method was used for estimating resistivity of

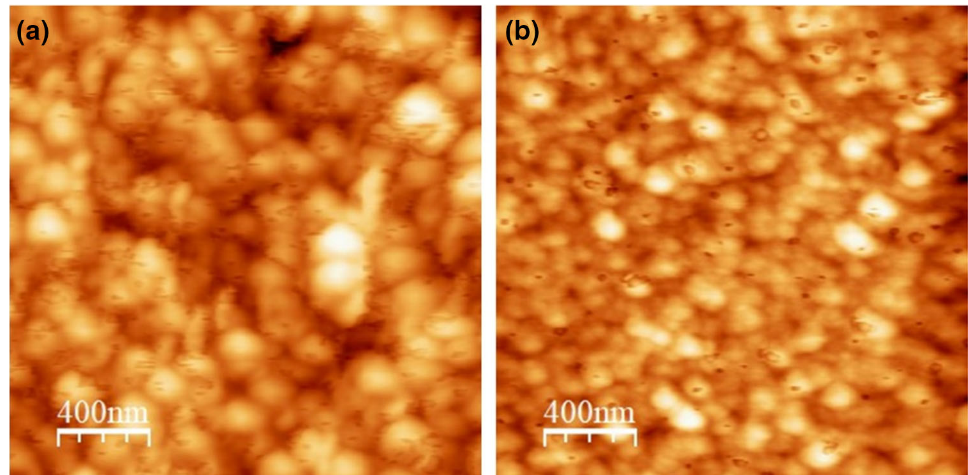

Fig. 6 AFM micrographs of $[GaSb/Mn]_3$ multilayer at **a** Ts = 293 K and **b** Ts = 423 K

Table 1 Thickness, Roughness Media Square (RMS), and grain sizes of $[GaSb/Mn]_n$ multilayers

Sample	Ts	Thickness (nm)	Roughness (nm)	Grain sizes (nm)
$[GaSb/Mn]_3$	293	300.42 ± 9.01	6.28 ± 0.13	180.08 ± 3.24
$[GaSb/Mn]_3$	423	327.27 ± 9.82	1.47 ± 0.03	129.48 ± 3.88
$[GaSb/Mn]_6$	293	470.31 ± 14.11	3.82 ± 0.07	131.87 ± 3.96

$[GaSb/Mn]_3$ multilayer with Ts = 423 K. Four I-V measurements within the bias range [-5 V, + 5 V] were performed, as sketched in Fig. 3a, giving rise to an average slope of $\overline{R} = 9.69 \pm 0.07 \times 10^7 \Omega$. The set of measurements look quite similar, which is attributed to sample's homogeneity. Therefore, the correction factor f in Eq. (1) that allows to calculate sample's resistivity, ρ is close to unity.

$$\rho = \frac{\pi}{\ln 2} f t_s \overline{R}. \quad (1)$$

Estimation of the resistivity requires the knowledge of sample thickness $t_s = 327.27 \pm 9.82$ nm. Replacing the values of all parameters in Eq. 1 results in a resistivity of $\rho = 3.40 \pm 0.11 \times 10^4 \Omega cm$.

The standard configuration for the Hall effect measurements using four-point contacts distributed on a square is shown in inset of Fig. 3b. The distance

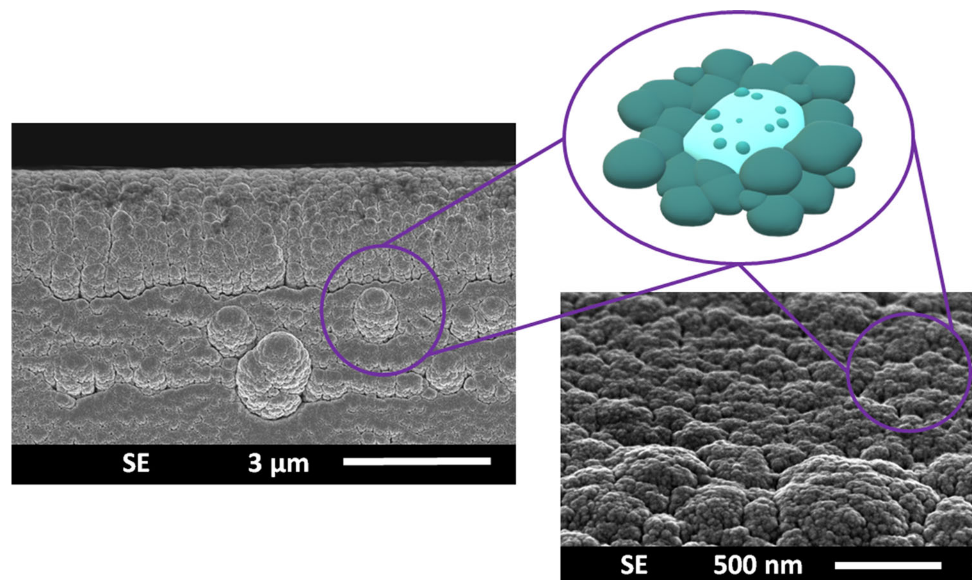

Fig. 7 HR-SEM micrographs of the surface of $[GaSb/Mn]_6$ multilayer on Si (100) at Ts = 293 K. Left, cross section of the sample; right, image on the surface; top-right, schematic diagram of the topography

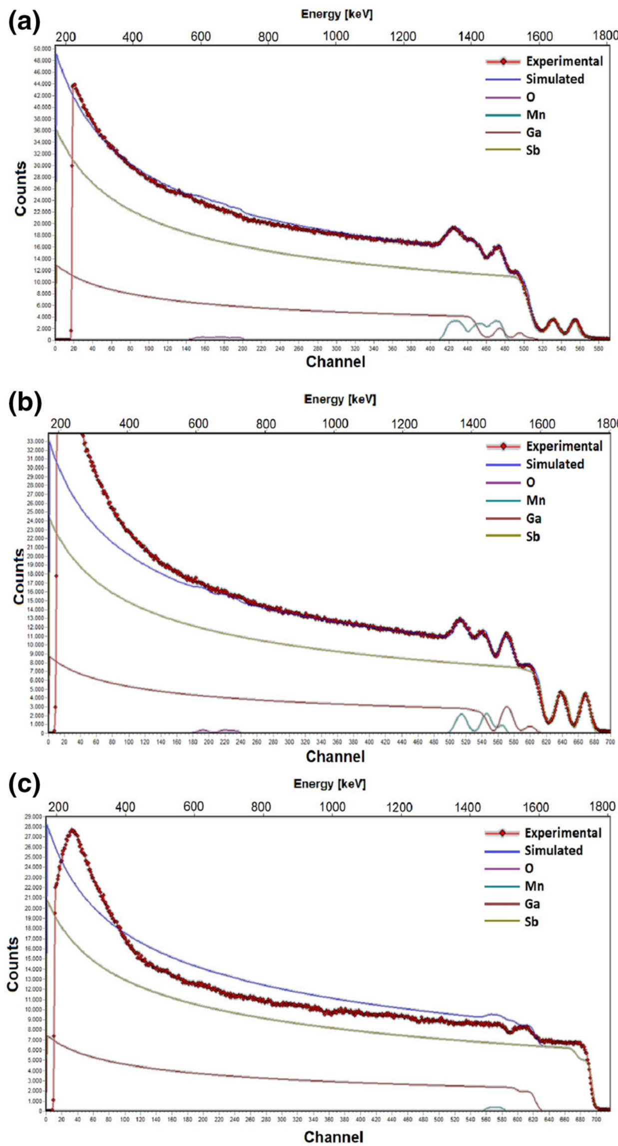

Fig. 8 Experimental (dotted lines) and simulated (straight lines) RBS spectra of multilayers: **a** $[GaSb/Mn]_3$ at Ts = 293 K, **b** $[GaSb/Mn]_3$ at Ts = 423 K, and **c** $[GaSb/Mn]_6$ at Ts = 293 K

between adjacent contacts is nearly 4 mm. Measurements were performed without and under an applied magnetic field $B = 1.09 \pm 0.05T$, oriented as sketched in inset of Fig. 3b. The current flux, shown in inset, resulted in a positive Hall voltage. Thus, holes are obtained like majority carriers in the film. Carrier density η is evaluated through Eq. 2.

$$\eta = \frac{B}{et_s}\frac{I}{V_H}. \tag{2}$$

Here, the ratio I/V_H (Hall conductance) is deduced from the slope of the I as a function of the Hall conductance (V_H) plot, which is depicted in Fig. 3b. Substitution of the corresponding measured parameters in Eq. 2 allows to estimate its carrier density to be $\eta = 4.14 \pm 0.17 \times 10^{13} cm^{-3}$, which evidences the p-type behavior of GaSb observed in the Raman measurements of Fig. 2.

In this way, it is possible to determine the Hall mobility μ_H is linked to conductivity through Eq. 3:

$$\sigma = e\eta\mu_H, \tag{3}$$

which the corresponding value was estimated as $\mu_H = 4.44 \pm 0.18 cm^2 V^{-1} s^{-1}$.

Morphological and topographical characterization was performed by HR-SEM and AFM measurements. Figure 4 shows the surface (with Secondary Electrons (SE) – right-up micrographs) and cross section (with Backscattering Electrons (BSE)—left-down micrographs) of $[GaSb/Mn]_3$ multilayer with Ts = 293 K. HR-SEM BSE micrographs evidenced the formation of the multilayer system characterized by GaSb (light gray) and Mn (dark gray) layers with columnar microstructure. Nevertheless, the surface layer presents a diffusion of the last GaSb and Mn layers may be associated with the high superficial mobility of the species and the phases instability due to the low substrate temperature.

When Ts was increased to 423 K, the layers of $[GaSb/Mn]_3$ multilayer are more distinguishable from each other (bottom right micrograph Fig. 5). The columnar microstructures are observed in HR-SEM micrographs (left-down Fig. 5) associated with the substrate temperature. This effect is consistent with the Movcham, Demchysim, and Thorton model for thin films deposited via sputtering [20]. This model considers that Ts and melting point of the targets (Tm) rule through their ratio of the mobility of the species sticking the surface and the ulterior growth of the films. In this case, considering both Ts = 293 K and Ts = 423 K, and that the Tm for the GaSb target is 985 K and for Mn target is 1517 K, the formation zone is called the first zone or zone I ($0 < Ts/Tm < 0.1$) [26], which is characterized by thin columnar formation and smaller grains on the surface. However, the deposition time of the multilayers (20 min for each GaSb layer and 15 min for each Mn layer) favored the mobility and adhesion of the ions, allowing the increase of the columnar microstructure and grain sizes.

Table 2 The depth profile $[GaSb/Mn]_3$ multilayer on GaSb wafer at Ts = 293 K

	Layer	Concentration	Thickness—RBS ($10^{15} atoms/cm^2$)	Thickness—SEM (nm)
$[GaSb/Mn]_3$	1—Surface	Mn – 0.38 O – 0.57 Ga – 0.02 Sb – 0.03	440	30.54
	2	Ga – 0.25 Sb – 0.23 Mn – 0.24 O – 0.28	90	31.90
	3	Mn – 0.32 O – 0.62 Sb – 0.03 Ga – 0.03	460	51.87
	4	Ga – 0.24 Sb – 0.115 Mn – 0.11 O – 0.495	190	32.09
	5	Mn – 0.32 O – 0.62 Sb – 0.03 Ga – 0.03	550	65.33
	6	Ga – 0.41 Sb – 0.35 O – 0.10 Mn – 0.14	50	-
	7	Ga – 0.41 Sb – 0.35 O – 0.24	150	37.86

Figure 6 shows the AFM micrographs of $[GaSb/Mn]_3$ samples at Ts = 293 K and 423 K, where grain size decreases with increasing substrate temperature. This effect is due to sufficiently high kinetic energies achieved over a long deposition time, which reduced the surface mobility and resulted in a smaller grain size (see Table 1) [27]. However, the mobility of species and diffusion ions on the surface may increase due to the high deposition time, generating the nucleation process as overlapping grains (Fig. 6) modifying the roughness and grain size (Table 1).

Table 1 presents the relation between synthesis parameters of $[GaSb/Mn]_n$ multilayers and Roughness Media Square (RMS), thickness, and grain size. The variation of sample thicknesses correlates with the number of layers in the multilayer, while the grain size variation was associated with the diffusion process. On the other hand, the roughness was modified by changing the grain size and could be observed in the coarse-grained formation on the surface (Fig. 6). This behavior is because the nucleation barrier is bigger and the supersaturation is low, generating large but few nuclei [27].

In the case of the $[GaSb/Mn]_6$ sample at Ts = 293 K, it is possible to observe the grains nucleation on the surface and the formation of the large nuclei composed of smaller grains (right-down HR-SEM micrograph Fig. 7). The schematic diagram of the large nuclei according to the micrographs is presented in the top-right of Fig. 7.

To identify the formation of layers and interlayers due to species diffusion and distribution, RBS measurements were performed (Fig. 8). This figure shows the 2 MeV He^{2+} RBS spectra of the $[GaSb/Mn]_n$ multilayers when the Ts was 293 K and 423 K. The simulated RBS spectra allowed estimation of the layer

Table 3 The depth profile $[GaSb/Mn]_3$ multilayer on GaSb wafer at Ts = 423 K

	Layer	Concentration	Thickness—RBS ($10^{15} atoms/cm^2$)	Thickness—SEM (nm)
$[GaSb/Mn]_3$	1—Surface	Mn – 0.29 O – 0.64 Ga – 0.02 Sb – 0.05	100	48.77
	2	Ga – 0.12 Sb – 0.25 Mn – 0.11 O – 0.52	220	45.41
	3	Ga – 0.04 Sb – 0.25 Mn – 0.08 O – 0.63	50	–
	4	Mn – 0.41 Ga – 0.02 O – 0.57	290	53.81
	5	Mn – 0.11 Ga – 0.21 Sb – 0.20 O – 0.48	50	–
	6	Ga – 0.54 Sb – 0.29 O – 0.12 Mn – 0.05	230	52.10
	7	Ga – 0.08 Sb – 0.20 Mn – 0.08 O – 0.64	50	–
	8	Mn – 0.39 O – 0.58 Sb – 0.03	340	53.78
	9	Ga – 0.29 Sb – 0.29 Mn – 0.12 O – 0.30	50	–
	10	Ga – 0.41 Sb – 0.43 O – 0.16	270	67.22

formation, species diffusion, and layer depth profile (see Tables 2 and 3).

The RBS spectra are fitted by multiple dispersion of Ga, Sb, Mn, and O elements and layer thickness. In the region, between 1200 and 1800 keV, it is possible to observe a decrease in intensity and some steps or peaks of spectra associated with the layers of the samples (Fig. 8). According to this dispersion, the concentration of elements by layers is presented in Tables 2 and 3.

Considering this concentration, the presence of diffusion into layers associated with the high mobility of the species was determined. In the case of $[GaSb/Mn]_3$ multilayer at Ts = 293 K, the layers are still distinguishable without the presence of interlayers; while, in the case of $[GaSb/Mn]_3$ multilayer at Ts = 423 K, the presence of dilute interlayers between the GaSb and Mn layers was determined (Table 3).

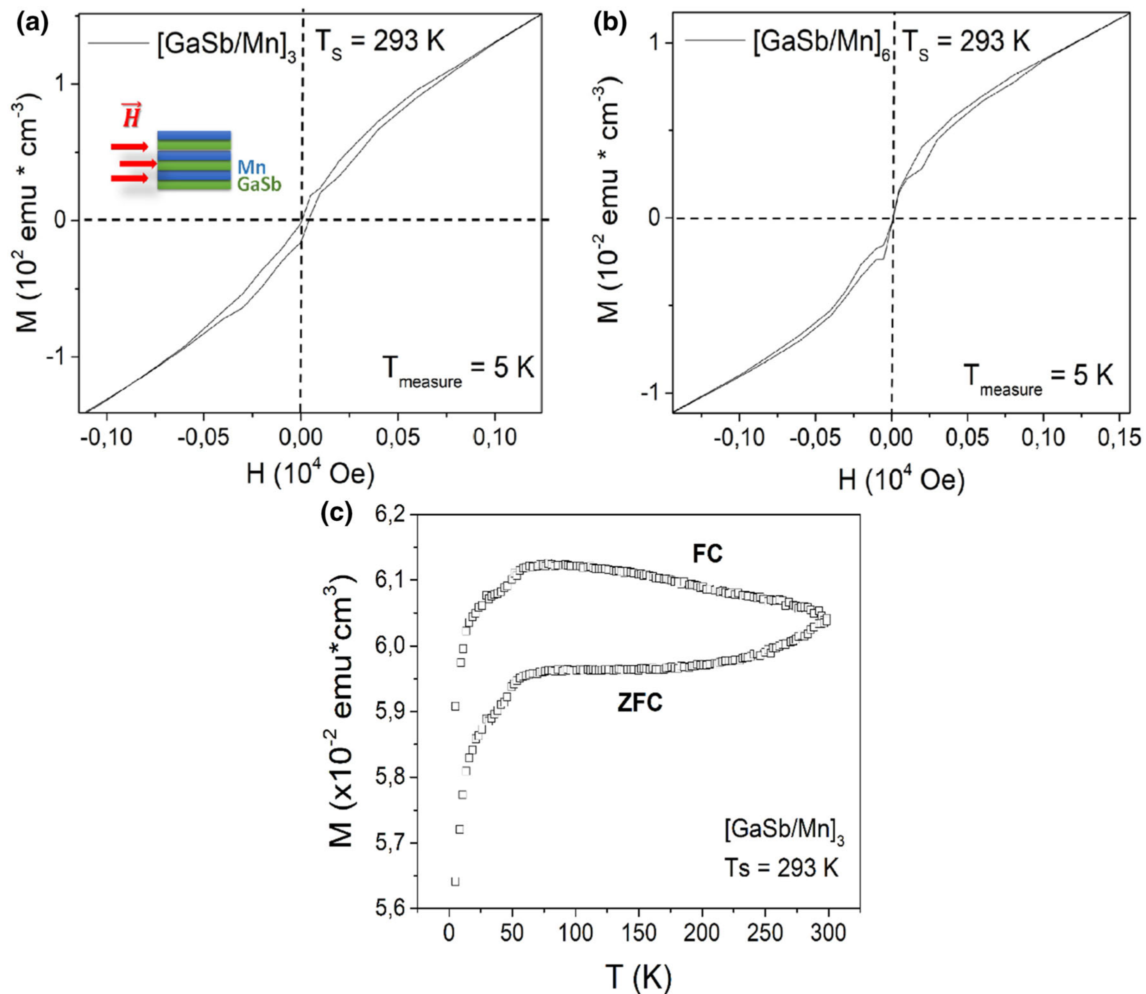

Fig. 9 Magnetization (M) as a function of applied magnetic field (H) at 5 K for **a** $[GaSb/Mn]_3$ multilayer on GaSb (100) at Ts = 293 K, **b** $[GaSb/Mn]_6$ multilayer on Si (100) at Ts = 293 K, and **c** ZFC–FC curves of $[GaSb/Mn]_3$ multilayer on GaSb (100) at Ts = 293 K

When the multilayer architecture is $[GaSb/Mn]_6$ at Ts = 293 K, the layer diffusion increases and the interlayers disappear (Fig. 8c). For this multilayer, the layer was characterized for 330 × 10^{15} atoms/cm^2 thickness of Ga, Sb, and Mn elements.

Figure 9 presents the magnetization (M) as a function of the applied magnetic field (H) at 5 K for $[GaSb/Mn]_3$ and $[GaSb/Mn]_6$, and ZFC–FC curves of $[GaSb/Mn]_3$ multilayers fabricated at room temperature. A ferromagnetic-like tendency was observed, which is associated with the formation of dilute interlayers observed in the RBS spectra. These interlayers may be contributing to magnetization as if they were small magnetic domains of the order of 50 × $10^{15} atoms/cm^2$ (see Table 3). However, the Mn layers have an antiferromagnetic behavior, which in competition with the diamagnetic GaSb layers, inhibit the saturation in the magnetization curves.

On the other hand, the shape of the hysteresis loop changes with the number of layers on the samples. The $[GaSb/Mn]_3$ multilayer presents the coercive field (Hc), but a small shift at high applied magnetic field, while in $[GaSb/Mn]_6$ the coercive field was reduced and loop curves are non-centrosymmetric. This behavior (ferromagnetic-like behavior) may occur when the magnetic anisotropy between the antiferromagnetic Mn layers and the formation of dilute ferromagnetic interlayer is larger than the interfacial exchange coupling [28, 29], in this case, mediated through GaSb layer, due to the $[GaSb/Mn]_n$ architecture.

Figure 9c presents ZFC–FC curves of $[GaSb/Mn]_3$ multilayer on GaSb (100) at Ts = 293 K. The

pronounced bifurcation of the FC and ZFC is observed at range temperature without a clear phase transition. This behavior can be associated with a contribution of dipolar and anisotropy magnetization, due to the competition of all the phases (GaSb, Mn, and Mn_2Sb_2 identified through XRD patterns), and layers present in the material.

4 Conclusion

The studies of $[GaSb/Mn]_n$ multilayers have shown the fabrication of this architecture at low substrate temperature via DC magnetron sputtering. Through Raman measurements, it was possible to establish the formation of p-type GaSb exhibiting a depletion surface space charge region due to the two coupled phonon–plasmon modes L_- and L_+. This behavior was corroborated by Hall measurements. HR-SEM results evidenced the multilayers architecture and columns formation in the microstructure, according to the synthesis method. Additionally, the grain size decreases with increasing substrate temperature due to sufficiently high kinetic energies obtained that reduce surface mobility. Diffusion and mobility of species were qualitatively derived from RBS spectra, in the formation of dilute interlayers, depending on the substrate temperature and the number of layers. Hysteresis loops and the sign of exchange bias effects due to the magnetic anisotropy and layer numbers were observed.

Acknowledgements

This work was supported by Universidad Nacional de Colombia. Jorge A. Calderón, scholarship of Doctorados Colciencias Conv. 785—2017. We acknowledge the service from the MiNa Laboratory at IMN, and funding from CM, MINECO and EU (FEDER, FSE).

Funding

This article was funded by Universidad Nacional de Colombia,MinCiencias,Con. 785,Jorge A. Calderón,MiNa Laboratory at IMN,CM,Miguel Manso Silván,MINECO,Miguel Manso Silván,EU (FEDER,Miguel Manso Silván,FSE), and Miguel Manso Silván.

Declarations

Conflict of interest The authors have not disclosed any competing interests.

References

1. H.P. Quiroz, M. Manso-Silván, A. Dussan, P. Carlos Busó-Rogero, F.M. Prieto, TiO_2 and Co multilayer thin films via DC magnetron sputtering at room temperature: Interface properties. Mater. Charact. **163**, 110293 (2020). https://doi.org/10.1016/j.matchar.2020.110293
2. B. Liu, Yu. Xiangjiang, X. Jiang, Yi. Qiao, Li. You, Y. Wang, F. Ye, Effect of deposition substrates on surface topography, interface roughness and phase transformation of the Al/Ni multilayers Appl. Surf. Sci. **546**, 149098 (2021). https://doi.org/10.1016/j.apsusc.2021.149098
3. A. Biswas, N. Abharana, S.N. Jha, D. Bhattacharyya, Non-destructive elemental depth profiling of Ni/Ti multilayers by GIXRF technique. Appl. Surf. Sci. **542**, 148733 (2021). https://doi.org/10.1016/j.apsusc.2020.148733
4. Z. Yuan, Y. Han, S. Zang, J. Chen, G. He, Y. Chai, Z. Yang, Fu. Qinqin, Analysis of the mechanical properties of TiN/Ti multilayer coatings using indentation under a broad load range. Ceram. Int. **47**, 10796–10808 (2021). https://doi.org/10.1016/j.ceramint.2020.12.196
5. G. Beainy, T. Cerba, F. Bassani, M. Martin, T. Baron, J.-P. Barnes, Suppression of self-organized surface nanopatterning on GaSb/InAs multilayers induced by low energy oxygen ion bombardment by using simultaneously sample rotation and oxygen flooding. Appl. Surf. Sci. **441**, 218–222 (2018). https://doi.org/10.1016/j.apsusc.2018.02.009
6. D. Datta, S.R. Bhattacharyya, T.K. Chini, M.K. Sanyal, Evolution of surface morphology of ion sputtered GaAs (100). Nucl. Instrum. Methods Phys. Res. B. **193**, 596–602 (2002). https://doi.org/10.1016/S0168-583X(02)00860-1
7. A. Wellner, R.E. Palmer, J.G. Zheng, C.J. Kiely, K.W. Kolasinski, Mechanisms of visible photoluminescence from nanoscale silicon cones. J. Appl. Phys. **91**(5), 3294–3298 (2002). https://doi.org/10.1063/1.1448394
8. K. Isobe, R. Okino, K. Hanamura, Spectral absorptance of a metal-semiconductor-metal thin-multilayer structured thermophotovoltaic cell. Opt. Express **28**, 40099–40111 (2020). https://doi.org/10.1364/OE.410828
9. J.-S. Liu, Y. Zhu, P.S. Goley, M.K. Hudait, Heterointerface engineering of broken-gap InAs/GaSb multilayer structures.

ACS Appl. Mater. Interfaces **7**, 2512–2517 (2015). https://doi.org/10.1021/am507410b
10. Z. Li, Lu. Yegang, M. Wang, X. Shen, X. Zhang, S. Song, Z. Song, Controllable multilevel resistance state of superlattice-like GaSb/Ge2Te films for ultralong retention phase-change memory. J. Non-Cryst. Solids **481**, 110–115 (2018). https://doi.org/10.1016/j.jnoncrysol.2017.10.030
11. K.S.A. Motlan, E.M. Butcher, T.L. Goldys, Tansley, Multilayer GaSb/GaAs self-assembled quantum dots grown by metalorganic chemical vapor deposition. Mater. Chem. Phys. **81**, 8–10 (2003). https://doi.org/10.1016/s0254-0584(03)00163-9
12. J.A. Calderón, A. Dussan, Thermal annealing effect on GaSb thin films deposited on Si (001) for assembly of GaSb/Mn multilayer systems at room temperature. J. Electron. Mater. **50**(11), 6403–6413 (2021). https://doi.org/10.1007/s11664-021-09161-7
13. F.Z. Meharrar, A. Belfar, I. Aouad, E. Giudicelli, Y. Cuminal, H. Aït-kaci, Analysis of the GaSb-p+/GaSb-p/GaSb-n+/GaSb-n structure performances at room temperature, for thermo-photovoltaic applications. Opt. **175**, 138–147 (2018). https://doi.org/10.1016/j.ijleo.2018.08.125
14. E.A. Chusovitin, D.L. Goroshko, S.A. Dotsenko, S.V. Chusovitina, A.V. Shevlyagin, N.G. Galkin, A.K. Gutakovskii, GaSb nanocrystals grown by solid phase epitaxy and embedded into monocrystalline silicon. Scripta Mater. **136**, 83–86 (2017). https://doi.org/10.1016/j.scriptamat.2017.04.004
15. K.S.A. Motlan, E.M. Butcher, T.L.T. Goldys, Multilayer GaSb/GaAs self-assembled quantum dots grown by metalorganic chemical vapor deposition. Mater. Chem. Phys. **81**, 8–10 (2003). https://doi.org/10.1016/S0254-0584(03)00163-9
16. C. Guo, Y. Sun, Z. Jia, Z. Jiang, Y. Lv, H. Hao, Xi. Han et al., Visible-extended mid-infrared wide spectrum detector based on InAs/GaSb type superlattices (T2SL). Infrared Phys. Technol. **89**, 147–153 (2018). https://doi.org/10.1016/j.infrared.2017.12.020
17. T.D. Golding, J.A. Dura, W.C. Wang, J.T. Zborowski, A. Vigliante, H.C. Chen, J.R. Meyer, Molecular beam epitaxial growth of Sb/GaSb multilayer structures: potential application as a narrow bandgap system. J. Cryst. Growth **127**, 777–782 (1993). https://doi.org/10.1016/0022-0248(93)90731-B
18. A.V. Kudrin, V.P. Lesnikov, D.A. Pavlov, Yu.V. Usov, Yu.A. Danilov, M.V. Dorokhin, Formation of epitaxial p-i-n structures on the basis of (In, Fe)Sb and (Ga, Fe)Sb diluted magnetic semiconductors layers. J. Magn. Magn. Mater. **487**, 165321 (2019). https://doi.org/10.1016/j.jmmm.2019.165321
19. M. Mayer, Application of accelerators in research and industry, Pts 1 and 2. AIP Conf. Proc. **475**, 541–544 (1999). https://doi.org/10.1063/1.59188
20. J. Maslar, W. Hurst, C.A. Wang, Raman spectroscopy of n-type and p-type GaSb with multiple excitation wavelengths. Appl. Spectrosc. **61**, 1093–1102 (2007). https://doi.org/10.1366/000370207782217789
21. J. Maslar, W. Hurst, C.A. Wang, Spectroscopic determination of electron concentration in n-type GaSb. J. Appl. Phys. **104**, 103521 (2008). https://doi.org/10.1063/1.3021159
22. , C. E. M. Campos, P. S. Pizani, Morphological studies of annealed GaAs and GaSb surfaces by micro-Raman spectroscopy and EDX microanalysis. Appl. Surf. Sci. **200**, 111–116 (2002). https://doi.org/10.1016/s0169-4332(02)00617-7
23. Y.L. Casallas-Moreno, M. Ramírez-López, G. Villa-Martínez, A.L. Martínez-López, M. Macias et al., Effect of the Sb content and the n- and p-GaSb (100) substrates on the physical and chemical properties of $InSb_xAs_{1-x}$ alloys for mid-infrared applications: Analysis of surface, bulk and interface. J. Alloys Compd. **861**, 157936 (2021). https://doi.org/10.1016/j.jallcom.2020.157936
24. A. Lahiri, N. Borisenko, M. Olschewski, R. Gustus, J. Zahlbach, F. Endres, Electroless deposition of III–V semiconductor nanostructures from ionic liquids at room temperature. Angew. Chemie - Int. Ed. **54**(11870–11874), 2015 (2015). https://doi.org/10.1002/anie.201504764
25. K. Sato, E. Saitoh, *Spintronics for Next Generation Innovative Devices* (John Wiley & Sons Ltd, West Sussex, United Kingdom, 2015)
26. B.C. Johnson, J.C. McCallum, M.J. Aziz, *Handbook of Crystal Growth: Thin Films and Epitaxy* (Elsevier North-Holland, Boston, 2015)
27. José M. Albella (2003) Láminas Delgadas y Recubrimientos, Preparación, propiedades y aplicaciones, Consejo Superior de Investigaciones Científicas, Spain, Madrid.
28. K. Wasa, M. Kitabatake, H. Adachi, *Thin Film Materials Technology: Sputtering of Compound Materials* (Springer Verlag, New York, 2004)
29. S.N. Sofronova, N.V. Kazak, E.V. Eremin, E.M. Moshkina, A.V. Chernyshov, A.F. Bovina, J. Alloys Comp. **864**, 158200 (2021). https://doi.org/10.1016/j.jallcom.2020.158200
30. A.G. Kolesnikov, M.E. Stebliy, A.V. Davydenko, A.G. Kozlov, I.S. Osmushko, V.V. Korochentsev et al., Magnetic properties and the interfacial Dzyaloshinskii-Moriya interaction in exchange biased $Pt/Co/Ni_xO_y$ films. Appl. Surf. Sci. **543**, 148720 (2021). https://doi.org/10.1016/j.apsusc.2020.148720

Publisher's Note Springer Nature remains neutral with regard to jurisdictional claims in published maps and institutional affiliations.